Physics in Medicine & Biology

PAPER • **OPEN ACCESS**

Impact of intense x-ray pulses on a NaI(Tl)-based gamma camera

IOP Publishing Phys. Med. Biol. 63 (2018) 065006 (12pp) https://doi.org/10.1088/1361-6560/aaaf02

Physics in Medicine & Biology

IPEM Institute of Physics and Engineering in Medicine

OPEN ACCESS

PAPER

Impact of intense x-ray pulses on a NaI(Tl)-based gamma camera

W J C Koppert, S van der Velden, J H L Steenbergen and H W A M de Jong

University Medical Centre, Utrecht, Netherlands

E-mail: w.j.c.koppert@umcutrecht.nl

Keywords: SPECT, PMT, NaI(Tl), gamma camera, real-time hybrid imaging

RECEIVED
21 August 2017

REVISED
11 January 2018

ACCEPTED FOR PUBLICATION
13 February 2018

PUBLISHED
14 March 2018

Abstract

In SPECT/CT systems x-ray and γ-ray imaging is performed sequentially. Simultaneous acquisition may have advantages, for instance in interventional settings. However, this may expose a gamma camera to relatively high x-ray doses and deteriorate its functioning. We studied the NaI(Tl) response to x-ray pulses with a photodiode, PMT and gamma camera, respectively.

First, we exposed a NaI(Tl)-photodiode assembly to x-ray pulses to investigate potential crystal afterglow. Next, we exposed a NaI(Tl)-PMT assembly to 10 ms LED pulses (mimicking x-ray pulses) and measured the response to flashing LED probe-pulses (mimicking γ-pulses). We then exposed the assembly to x-ray pulses, with detector entrance doses of up to 9 nGy/pulse, and analysed the response for γ-pulse variations. Finally, we studied the response of a Siemens Diacam gamma camera to γ-rays while exposed to x-ray pulses.

X-ray exposure of the crystal, read out with a photodiode, revealed 15% afterglow fraction after 3 ms. The NaI(Tl)-PMT assembly showed disturbances up to 10 ms after 10 ms LED exposure. After x-ray exposure however, responses showed elevated baselines, with 60 ms decay-time. Both for x-ray and LED exposure and after baseline subtraction, probe-pulse analysis revealed disturbed pulse height measurements shortly after exposure. X-ray exposure of the Diacam corroborated the elementary experiments. Up to 50 ms after an x-ray pulse, no events are registered, followed by apparent energy elevations up to 100 ms after exposure. Limiting the dose to 0.02 nGy/pulse prevents detrimental effects.

Conventional gamma cameras exhibit substantial dead-time and mis-registration of photon energies up to 100 ms after intense x-ray pulses. This is due PMT limitations and due to afterglow in the crystal. Using PMTs with modified circuitry, we show that deteriorative afterglow effects can be reduced without noticeable effects on the PMT performance, up to x-ray pulse doses of 1 nGy.

1. Introduction

Hybrid imaging systems, such as single photon emission computed tomography (SPECT)/CT and positron emission tomography (PET)/CT, provide combined anatomical and molecular information. Conventionally, the nuclear and x-ray images are acquired in sequence. However, simultaneous acquisition may have specific advantages, for instance to prevent registration errors due to movement between the x-ray acquisition and nuclear imaging. This may be important for high quality diagnostics but also when using hybrid imaging in an interventional setting.

Single modality imaging systems, such as x-ray computed tomography (CT) and handheld gamma cameras, are successfully used in the intervention room in clinical practice (Raj *et al* 2013, Vidal-Sicart *et al* 2014). However, no molecular information is provided in x-ray CT images, whilst gamma cameras lack anatomical information. A combination of x-ray and nuclear imaging could be valuable in guided interventions. A particular example of a procedure that could greatly benefit from such a combination is radioembolisation with Yttrium-90 (^{90}Y) microspheres of unresectable liver tumours (Braat *et al* 2015). Availability of live hybrid images can potentially be used to assess lung shunt fraction and extrahepatic depositions, possibly obviating imaging at the nuclear medicine department. Besides radioembolisation, biopsies and sentinel node procedures are examples of possible applications (Kobayashi *et al* 2012, Shyn 2013).

In a simultaneous setting, however, the gamma camera may be exposed to a substantial amount of x-rays. As an example, we tested earlier a prototype hybrid C-arm capable of acquiring simultaneous, real-time fluoroscopic and nuclear images of the same field-of-view (FOV) (Beijst *et al* 2016, van der Velden *et al* 2017). Feasibility of acquiring simultaneous fluoroscopic and nuclear images with good spatial and temporal overlap was shown with phantom experiments.

It was, however, also observed that an excessive number of counts was detected in the 140 keV energy window in presence of x-rays (Beijst *et al* 2016). This effect increased rapidly with growing tube voltages and the addition of scatter material. In additional measurements, we observed that the gamma camera was unable to measure any γ-rays during or directly after an x-ray pulse. These effects limit the performance of a hybrid x-ray/nuclear imaging device to small x-ray doses only.

Gamma cameras are designed for energy resolved counting of individual photons with energies in the range of 50–500 keV. The counting performance of gamma cameras is often expressed in terms of counts per second (cps) both for sensitivity, count rate and for dead-time. Dead-time of a gamma camera is typically small below 2×10^5 cps. Above this, pulse pile-up is reported (Cherry *et al* 2012), while much higher count rates cannot be handled by the gamma camera and cause blindness. Rather than counts, the performance and exposure of x-ray detectors is often described in Gy. The typical dose required for formation of an x-ray image varies between 10 nGy (low quality fluoroscopy frame) and 1 μGy (high quality diagnostic x-ray). The typical exposure time is 10 ms per frame. To put this in perspective for a gamma camera, a dose of 10 nGy (i.e. low quality fluoroscopy frame) during 10 ms is equivalent to 10^{10} cps at 80 kV tube voltage, which is approximately 10^5 higher than the count rate that can be handled by a gamma camera without dead-time.

It is unknown to what extent such high x-ray doses affect the performance of the gamma camera during and directly after exposure. One effect that has been reported frequently after x-ray exposure of a scintillator is called afterglow (Koički *et al* 1973, Gobain 2018, Rodnyi 1997). Afterglow is phosphorescence due to thermal release of charges from traps in a scintillation crystal. Although this effect has been described in detail for scintillators used in x-ray detection, little is known of afterglow effects in a NaI(Tl)-based gamma camera.

Therefore, the first purpose of this study is to evaluate the performance of a gamma camera in the presence of a burst of x-ray pulses with varying intensities. The problem is dissected by investigating a NaI(Tl) scintillator read out by a photodiode, a NaI(Tl)-PhotoMultiplier Tube (PMT) assembly exposed to LED light and a single NaI(Tl)-PMT assembly exposed to a burst of x-ray pulses. In addition exposure of a conventional gamma camera gives the response of an ensemble of PMTs with standard processing. The second purpose is to study potential modifications in the electronic circuitry, to improve the performance in presence of x-rays.

2. Methods

Four different set-ups were used to investigate the impact of x-ray pulses on a NaI(Tl) gamma camera. First, an isolated NaI(Tl) scintillation crystal was read out using a photodiode to measure potential afterglow. Next, a PMT was exposed to LED light, mimicking the response of the scintillation crystal, to study the isolated PMT response. Furthermore, a NaI(Tl)-PMT assembly was exposed to x-rays to study the combined PMT and scintillation crystal response. Finally, the response of a clinical gamma camera to x-ray pulses was studied.

2.1. Afterglow

A NaI(Tl) crystal was optically attached to a Hamamatsu s1227 Silicon photodiode. The assembly was exposed to a 120 kV, 100 mA x-ray pulse for the time of one second at a Focus-to-Detector-Distance (FDD) of 80 cm, which is equivalent to a dose of 20 mGy. The photodiode signal was amplified by a current-to-voltage convertor (HMS Model 564) and sampled at 10 kHz by a 15 bit ADC.

2.2. PMT response to a LED pulse

To isolate the problem of PMT effects, a Scionix 51B51/2M-Neg NaI(Tl)-PMT (ETL 9266B (ET Enterprises 2010)) assembly, 10 dynodes, 5.1 cm in diameter, was internally exposed to a 10 ms ('main pulse') red LED pulse from the socket side to mimic light output from a NaI(Tl) scintillator due to an x-ray pulse. In addition, to avoid dependence of the stochastic nature of a radioactive source, we probed the PMT performance by exposing it to a burst of short LED flashes at 10 kHz ('probe pulses') with a pulse intensity that is approximately equivalent to the scintillator response to a 122 keV ^{57}Co photon.

Ideally, we would have used a conventional blue LED which is closer to the NaI(Tl) emission spectrum. However, limited by the clock frequency of our 16.5 MHz pulse generator electronics, we could only generate pulse lengths with a integer factor of 62.5 ns. A conventional blue LED pulse of this pulse length would have induced a signal more than an order of magnitude larger than a 122 keV gamma photon. We therefore decided to use a red LED, since the PMT is less sensitive for this wavelength. A pulse length of 312.5 ns was found to give signals that are comparable to 110 keV gamma signals. Assuming a linear LED response, it was calculated that the PMT

response to a 10 ms LED pulse is equivalent to the response of 32×10^3 110 keV gamma photons in the same time. Such a LED pulse has a simulated total absorbed energy that is comparable to a 0.7 nGy pulse at 80 kVp (mean energy 72.8 keV) over the full crystal surface.

We performed two measurements per setting; first, we measured the response to the main pulse only, then we measured the response of the main pulse followed by the probe pulse burst. Subtraction of both yields the isolated probe pulse response, ruling out any direct effects caused by the main LED pulse.

A PMT consists of a number of dynodes in series connected to a voltage divider. Our PMT was connected using a voltage divider circuitry as recommended by ET enterprises (ETL) (ET Enterprises 2010) with capacitors connected in parallel to the last three dynodes. In our experiments we studied two different capacitances; conventionally used 10 nF and 1 nF, the latter choice is clarified below.

As a rule of thumb, linearity is assured when the maximum charge contained by the capacitors is at least 100 times larger than the charge (or current) that is generated in the amplification process (Photomultiplier Tubes Basics and Applications 3a, Hamamatsu 2007), as is expressed by the condition:

$$C_{\text{min}} = 100\ Q/V. \tag{1}$$

The output pulse charge Q of an ideal PMT, as result of an interacting gamma with energy E_γ in the crystal, can be expressed as (Photonis (2002) and Knoll (2000)):

$$Q = YE_\gamma C_{\text{eff}} Q_{\text{eff}} Ge. \tag{2}$$

Here the photon yield for NaI(Tl) scintillation crystals $Y = 38$ photons keV^{-1} (Gobain 2018), the gamma energy $E_\gamma = 122$ keV, the electron collection efficiency $C_{\text{eff}} \approx 0.8$ (Photonis 2002), the cathode quantum efficiency $Q_{\text{eff}} \approx 0.3$ (ET Enterprises 2010), the PMT gain $G \approx 10^5$ at 600 V (ET Enterprises 2010) and e is the elementary charge. For the latter values, equation (2) yields 18 pC per 122 keV pulse. For a potential difference of $V = 50$ V over the capacitors (e.g. a cathode voltage of -600 V) and 1 nF capacitors, condition (1) is satisfied.

Exposure of the PMT to intense light will result in discharged capacitors, requiring a charge-up time τ before the gain restores to its nominal value. Equation (3) shows the expression for the charge-up time τ of a capacitor for a given capacitance C and resistance R.

$$\tau = RC. \tag{3}$$

For our application we require a charge-up time of $\tau < 1$ ms after an x-ray pulse. For 470 kΩ resistors in our resistor chain and 1 nF capacitors this condition is satisfied as well.

The effects of discharged capacitors are directly affected by the PMT gain, which is a function of the cathode voltage, therefore the measurements are also performed at different cathode voltages: -500 V and -600 V. Summarising we performed the following measurements: (1) 1 nF, -500 V; (2) 1 nF, -600 V; (3) 10 nF, -500 V; (4) 10 nF, -600 V; and studied the differences.

The PMT cathode is directly coupled to the high voltage power supply that remains stable during the main pulse. Hence a voltage drop on the cathode, as induced by discharged capacitors is avoided. This is desired since the cathode has a large surface resistivity possibly giving rise to additional recovery times.

For the experiments, the raw PMT responses were measured by a Picoscope oscilloscope terminated with a 1 MΩ resistance, no active amplification was required. The raw waveform was sampled at 10 MHz, the signals were integrated offline to acquire a measure of the gamma energy in ADC counts. This value was linearly transformed to equivalent energy (in keV) by an offset correction and a scaling factor that were extracted from calibration measurements based on ^{57}Co and ^{99m}Tc exposure.

2.3. X-ray pulse response of a NaI(Tl)-PMT assembly

In this section, we study the response of a NaI(Tl)-PMT assembly on an x-ray pulse, thereby enabling the presence of afterglow. The PMT is now exposed to x-ray pulses from a Philips Veradius C-arm. The x-ray tube voltage and current are set at 80 kV and 1.68 mA, respectively. The x-ray pulses have a length of about 9.6 ms with a pulse rate of 15 Hz.

Two cases are studied; exposure of the detector to a dose of 1 nGy, by using a 7 mm Cu filter and exposure to a dose of 9 nGy, by using a 4.6 mm Cu filter. In analogy to the previous experiment, the PMT is probed during and after exposure using LED probe pulses generating signals that are approximately equivalent to one 122 keV gamma interaction. Figure 1 shows a picture of the set-up.

We performed four different measurements at varying capacitances and cathode voltages: (1) 1 nF, -500 V; (2) 1 nF, -600 V; (3) 10 nF, -500 V; (4) 10 nF, -600 V. In each measurement we exposed the detector to three consecutive x-ray pulses and we measured the detector response as well as the cathode and dynode voltages. Similar to the method used in the previous section, we subtract the probed from the unprobed response yielding the isolated gamma waveforms. From these the gamma energies were acquired.

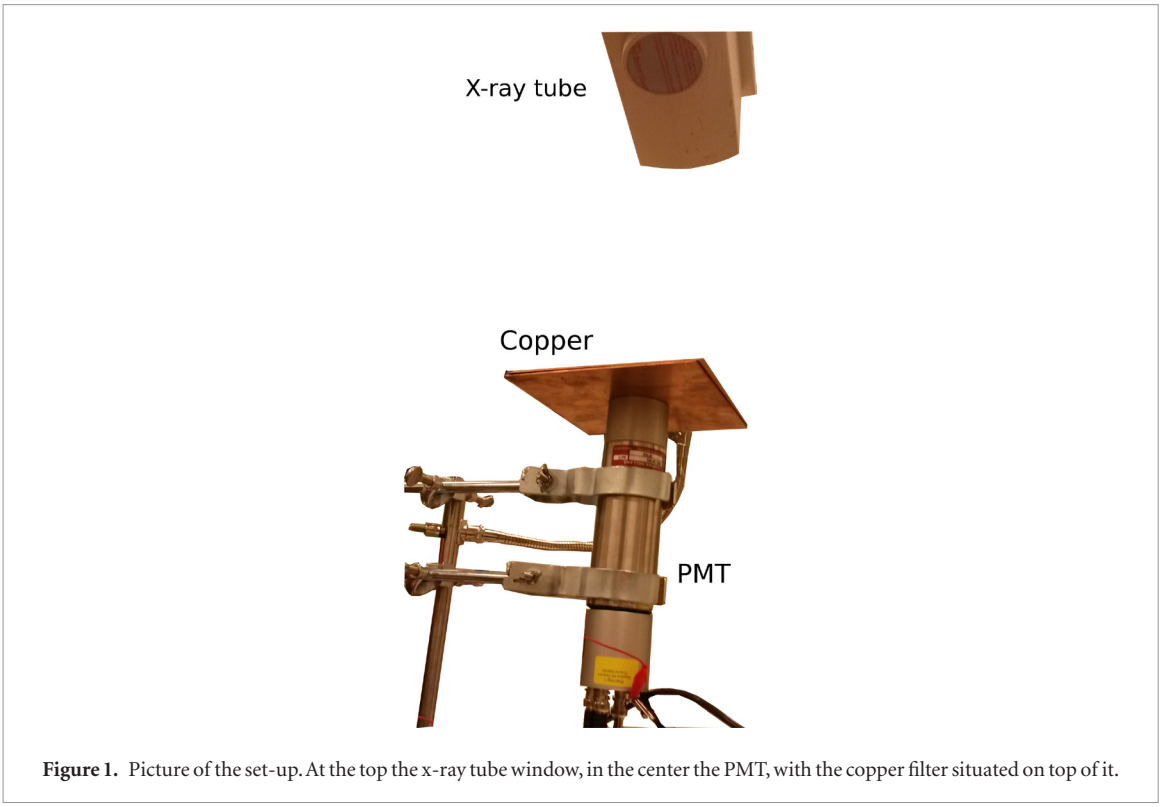

Figure 1. Picture of the set-up. At the top the x-ray tube window, in the center the PMT, with the copper filter situated on top of it.

2.4. Gamma camera response to x-ray pulse burst

A Diacam gamma camera (Siemens, Erlangen, Germany) was used to study the behavior of a conventional gamma camera during and after x-ray exposure. All experiments were performed in absence of a collimator, to avoid collimator dependent results. The gamma camera was exposed to several bursts of x-ray pulses of different intensities, to find the maximum x-ray dose the gamma camera could handle without deterioration. Furthermore we studied any effects appearing beyond this dose.

Due to limited availability and different from the previous experiments, here an x-ray tube of a Philips BV-29 C-arm in fluoroscopy mode is used, instead of a Philips Veradius x-ray tube, to generate a continues x-ray flux in a circular Field of View (FoV) on the gamma camera with a 23 cm diameter at 1 m FDD. The tube has been modified with a mechanical chopper to generate short x-ray pulses with similar properties to a modern conventional fluoroscopic device i.e. a pulse length of 15 ms at 15 Hz repetition rate with a trapezial shape. The x-ray tube voltage and current were set to 80 kV and 2.8 mA, respectively. We exposed the gamma camera to a burst of nine x-rays pulses to study the response after each consecutive pulse. The gamma camera response measurements were performed at several doses ranging from 0.02 nGy to 6.6 nGy, by attenuating the x-ray beam with copper filters of varying thicknesses. Dose per pulse measurements were performed by an Unfors Raysafe situated in the centre of the FOV of the Gamma Camera. Outside the primary FOV, the gamma camera was shielded to minimize the effect of scattered x-rays. Figure 2 visualises the set-up. The gamma camera was read out in listmode. Instead of using a LED probe pulse, here we measured the γ-ray counting performance during and after x-ray exposure using a ^{57}Co (122 keV) with an activity of 2.2 MBq situated in the FOV at a distance of 60 cm from the gamma camera.

3. Results

3.1. Afterglow

Figure 3 shows the photodiode response normalised to the x-ray signal height as function of time. The afterglow signal level after 3 ms is about 15% in our NaI(Tl)-photodiode assembly. This fraction is somewhat large compared to Koički *et al* (1973) reporting decay times of 150 ms containing 9% of the signal, but much larger than 5% at 6 ms as has been reported by Gobain (2018). The figure indicates that the curve can be approximated by a sum of three exponentials in the first 500 ms. The two most important time scales are 168 and 55 ms, of which the latter is dominant in the time range (up to 200 ms) that we study in this paper. The 3 ms component has an amplitude that is a factor 20 less and much shorter than the timescales we study, therefore this is component is not of interest.

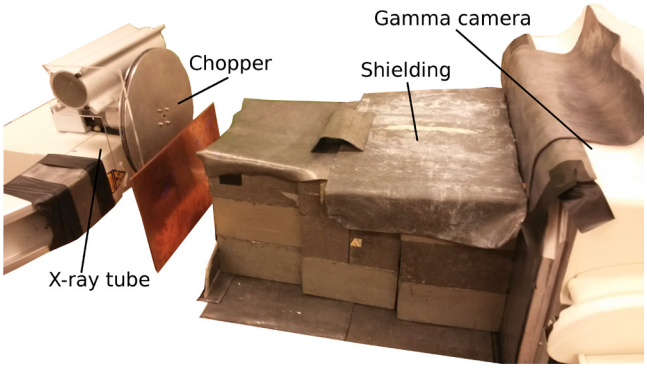

Figure 2. Picture of the experimental set-up. The x-ray tube is situated at the left, the shielded gamma camera at the right.

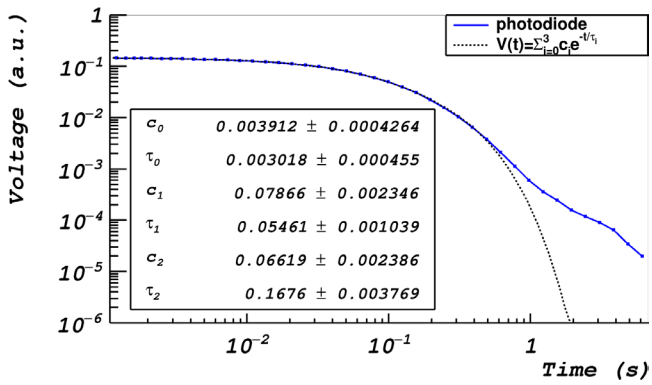

Figure 3. Afterglow intensity in NaI(Tl) as result of a high intensity x-ray pulse. The curve is fitted with a sum of three exponentials with three different decay times.

3.2. PMT response to a LED pulse

Figure 4 shows the voltages of most of the dynodes and the photocathode during the main (10 ms) LED pulse with 10 nF capacitors. It can be seen that the potential difference over the last dynodes (D9, D10) drops dramatically during the main pulse causing the potential difference between the other dynodes to increase. Furthermore, the inset in figure 4 shows that it takes more than 10 ms before the voltages on the last dynode (D10, magenta) are restored. For comparison, the inset in figure 4 shows the voltages of the last dynode (D10, black) in case of a 1 nF capacitor as well, showing a ten times faster recovery time after the end of the pulse.

Figure 5 shows the PMT response to a 10 ms LED pulse with (in blue) and without probe pulses (in red) for a cathode voltage of −600 V and 10 nF capacitors. Subtraction of both curves yields the green curve in figure 6, showing the amplitude as a measure for the detected photon energy. In addition, the figure shows the response amplitudes for a cathode voltage of −600 V with 1 nF capacitors, −500 V with 10 nF capacitors and −500 V with 1 nF capacitors, respectively.

3.3. X-ray pulse response of a NaI(Tl)-PMT assembly

3.3.1. Response to 1 nGy x-ray pulses

Figure 7 shows the voltages of the last four dynodes, during and after the x-ray exposure, in case of 10 nF capacitors and the voltage at the last dynode in case of 1 nF, all for a dose of 1 nGy with the cathode voltage at −600 V. The shape of the response is comparable with figure 4, however a subtle difference can be seen in the tails (indicated by the arrows). It seems that the baseline grows in amplitude after each pulse, this is believed to be the effect of afterglow in the NaI(Tl) crystal. Afterglow in NaI(Tl) contains timescales that are much longer than the time between two pulses, hence a build-up effect occurs. When the number of excited states as generated in the crystal during an x-ray pulse equals the number of states decaying between the pulses, the afterglow intensity reaches an equilibrium. It can be shown that given an exponential decay with a decay time of 70 ms at a pulse rate of 15 Hz, the baseline converges to a constant value in about 8 pulses. Figure 8 shows the probe pulse energies as measured with similar settings as the voltages in figure 7.

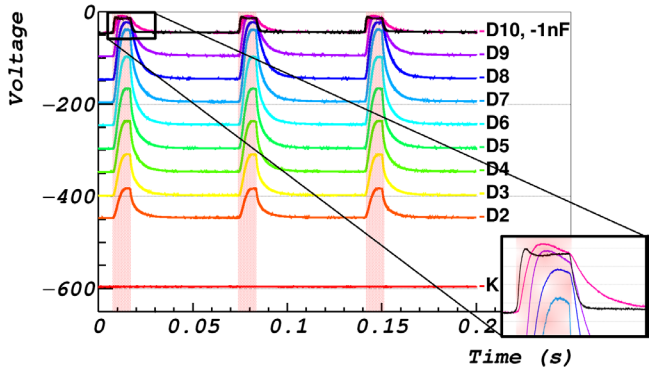

Figure 4. Voltages of the last nine dynodes and the photocathode during a 10 ms LED exposure in rainbow colors. The cathode voltage is -600 V, the capacitors have values of 10 nF. For comparison, the voltage of the last dynode (D10) in case of 1 nF capacitors at similar voltages is shown in black. The time that the LED pulse is turned on is indicated by the red hatched area.

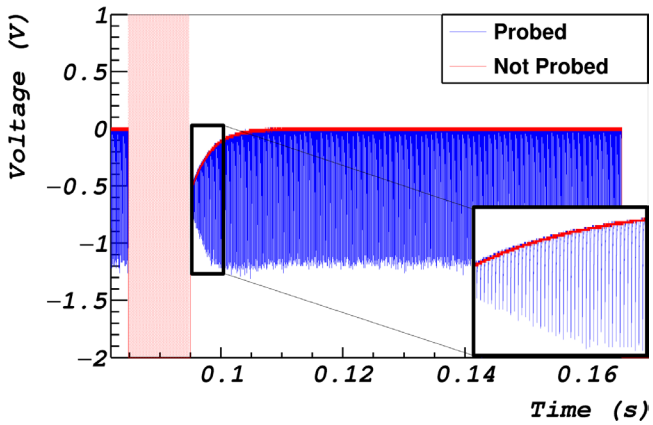

Figure 5. Raw PMT response as recorded with an oscilloscope. The PMT response to a 10 ms LED pulse with (in blue) and without probe pulses (in red). Individual probe pulses are hardly visible but the blue band shows the trend. The inset shows a closer look at individual pulses. The cathode voltage is −600 V, the capacitors have values of 10 nF. The time that the LED pulse is turned on is indicated by the red hatched area.

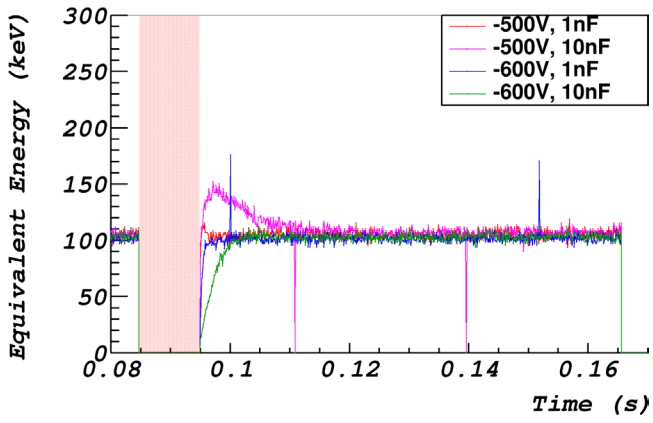

Figure 6. Amplitudes of the PMT response on LED probe pulses against time corresponding to 10 nF at −500 V, −600 V and 1 nF at −500 V, −600 V respectively. The time that the LED pulse is turned on is indicated by the hatched area. Note that the spikes in the curves are caused by background radiation.

3.3.2. Response to 9 nGy x-ray pulses

We exposed the PMT with 1 nF capacitors and cathode voltages of −500 V and −600 V to 9 nGy x-ray pulses to measure the dynode voltages and the PMT response. Figure 9 shows the dynodes voltages for −500 V cathode voltage, the build-up as mentioned in the previous section is better visible due to the large dose. Furthermore it can be seen that, in case of −600 V, there is a significant voltage drop over the capacitors after the first x-ray pulse. The voltages do not have time to recover before the next x-ray pulse appears. In addition figure 9 shows that the

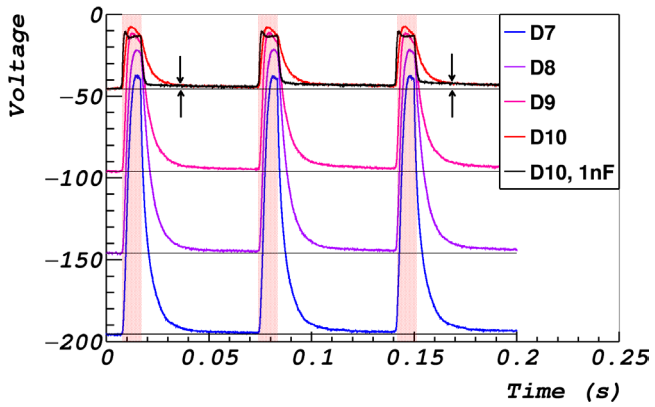

Figure 7. Voltages of the last four dynodes and the voltage of the last dynode in case of 1 nF (in grey) during and after 1 nGy x-ray exposure. The cathode voltage is −600 V the capacitors have values of 10 nF. The black lines indicate the nominal values of the dynodes, the arrows indicate a small elevation of the baseline due to build-up. The time that the x-ray pulse is turned on is indicated by the red hatched area.

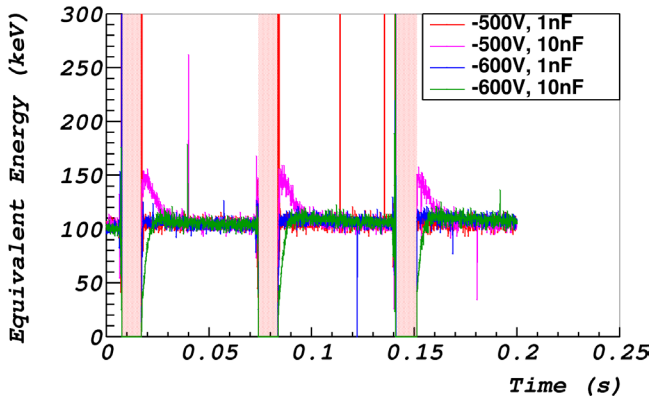

Figure 8. The measured energies versus time, corresponding to the settings in figure 6 but here exposed to x-ray pulses of 1 nGy.

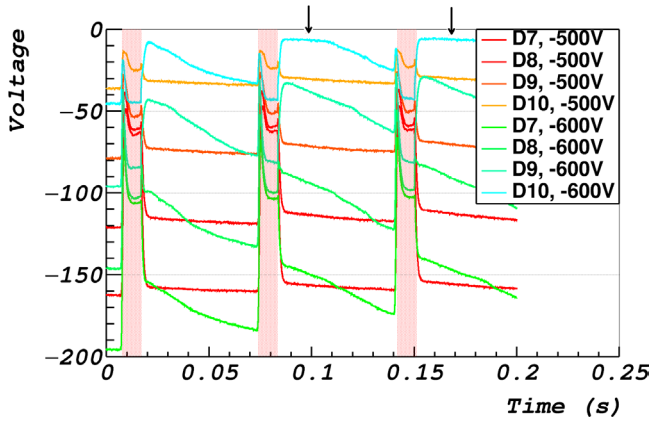

Figure 9. Dynode voltages of the last four dynodes with 1 nF capacitors at −500 V (red-like) and −600 V (green-like) cathode voltages during 9 nGy x-ray pulses.

voltage of D10, in case of −600 V cathode voltage, is constant for about 30 ms shortly after the second pulse and even longer for the third pulse.

For illustration, figure 10 shows the unprobed responses corresponding to the −500 V, 1 nF case, for different dose. The presence of afterglow and build-up can be seen, furthermore the afterglow tail of the 9 nGy curve seems to be about nine times more intense than the 1 nGy curve, showing that afterglow is proportional to the dose. Note that a probe LED pulse (or a 110 keV gamma) has an amplitude of about −0.25 V, which is small compared to afterglow signal in the 9 nGy case.

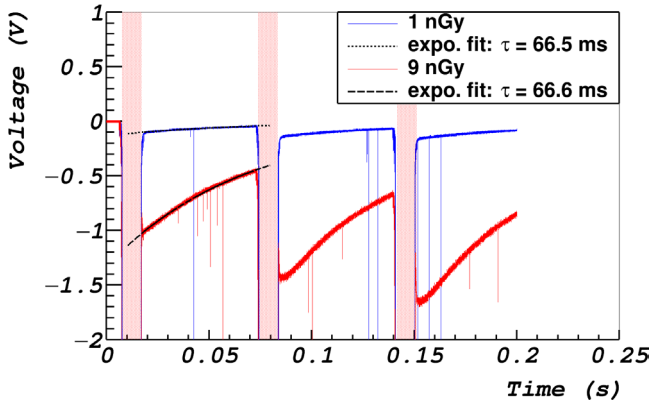

Figure 10. The unprobed PMT responses to 1 and 9 nGy x-ray pulses in case of −500 V cathode voltage and 1 nF capacitors. For comparison; a probe pulse has an amplitude of about −0.25 V. The fits show that both curves have a similar decay time of $\tau = 67$ ms.

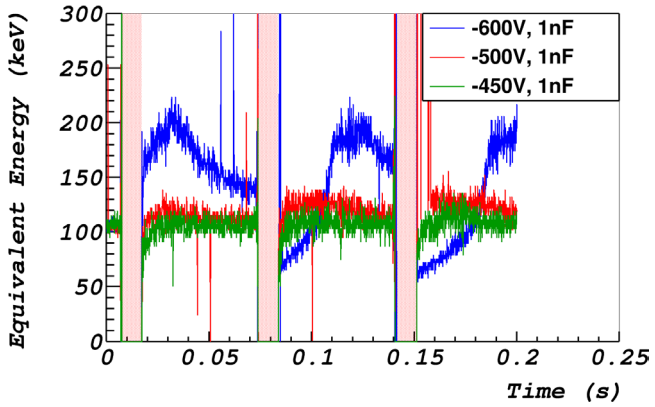

Figure 11. The measured energies corresponding to the settings in figure 9; 1 nF at a cathode voltage of −500 and −600 V. In addition the measured energies for −450 V cathode voltage.

Figure 11 shows the energies for cathode voltages of −600 V, −500 V and −450 V in the case of 1 nF capacitors. The energies of the −600 V curve are excessive after the first pulse. After the second pulse however, the energies are smaller than expected for a time that seems to be correlated with the time where the capacitor voltage is constant, as indicated by the arrows in figure 9. In the −500 V curve, the energies are closer to the expected value (e.g. 110 keV), but amplitudes appear to slightly increase in consecutive pulses. For comparison, a similar measurement is performed at −450 V, showing that the elevation of the measured energies decreases with gain.

3.4. Gamma camera response to x-ray pulse burst

Figure 12 shows a 2D histogram showing the reconstructed energy versus time for the last four (out of nine) x-ray pulses with a dose per pulse of 0.02 nGy. Every dot is a 2D bin, the colour indicates the number of photons in the bin. Clearly visible are the ^{57}Co counts at 122 keV. During the x-ray pulses, effects of pile-up can be observed with reconstructed energies as high as 300 keV.

Figure 13 shows a 2D histogram similar to the previous figure but here the Diacam is exposed to a 10 times higher x-ray dose of 0.28 nGy. In figure 12, an excess of counts at energies much higher than 122 keV is observed during the x-ray pulse (i.e. 0.59 to 0.60 s). Although these counts suffer from pile-up, they could be identified. With high x-ray doses, however, hardly any counts are recorded during the x-ray pulse, as is seen in figure 13. After exposure a sudden increase of the reconstructed energy of the ^{57}Co counts occurs, it relaxes to the nominal energies with a decay time of about 50 ms.

Figure 14 shows the case with an x-ray pulse dose of 1.14 nGy. Hardly any counts can be observed during the x-ray pulse and a period of about 40 ms afterwards. In addition a strong elevation in energy occurs, that shows up shortly after the end of the x-ray pulse. The latter seems to recover within 100 ms from the last pulse, comparable to figure 13. For 6.6 nGy per pulse the gamma camera was permanently blinded, therefore those results cannot be shown.

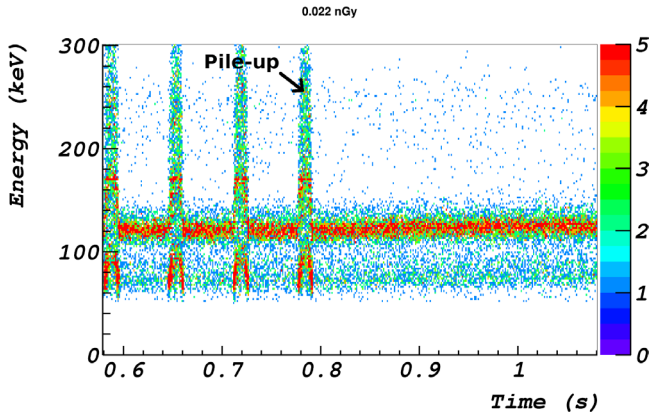

Figure 12. 2D histogram showing energy versus time of the last four x-ray pulses out of a burst of nine. Each pulse contains an x-ray dose of about 0.02 nGy. During the x-ray pulses pile-up effects can be observed, the gamma camera performs as expected in between the x-ray pulses.

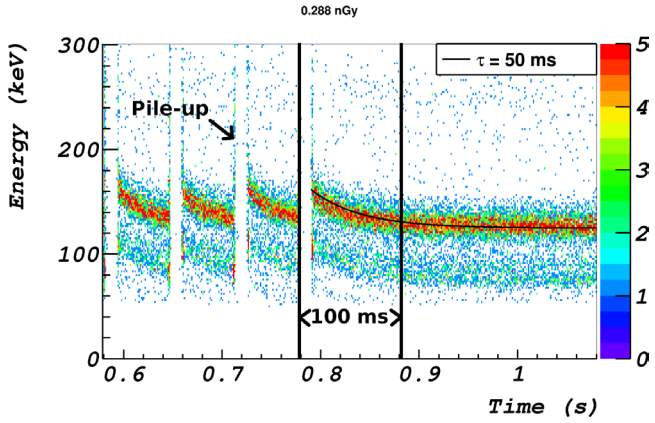

Figure 13. 2D histogram showing energy versus time of the last four x-ray pulses out of a burst of nine. Each pulse contains an x-ray dose of about 0.28 nGy. During the x-ray pulses pile-up effects as well as a reduced count rate can be seen, in between the x-ray pulses excessive reconstructed energies are measured. For comparison an exponential function with a decay time of 50 ms is shown on top of the data after the last pulse.

4. Discussion

This study reports on a number of experiments to analyse the effects of x-ray exposure on a traditional gamma camera. We showed that below a dose of 0.02 nGy per pulse, corresponding to 10^2 x-rays per cm^2 per pulse, only detrimental effects (elevated energies because of pile-up) can be observed during the x-ray pulses. At higher doses, non-linear effects were observed directly after the pulses. These effects could be explained in terms of afterglow and PMT limitations, by studying the response of an individual PMT-NaI(Tl) assembly to both LED and x-ray exposure.

4.1. Afterglow

The afterglow fraction in Na(Tl) is measured to be about 15% after 3 ms and contains time components from milliseconds up to several seconds. The fit in figure 3 suggests the presence of two dominant decay time components; 54 ms and 167 ms. The first component is comparable with the decay times as found with the NaI(Tl)-PMT assembly in figure 10 (67 ms) and with the gamma camera in figure 13 (50 ms). The second component could not be verified with the latter set-ups, since time scales are too long. The effect of the second component could be studied in a larger measurement sequence. The afterglow fraction seems to be somewhat large compared to Koički *et al* (1973) reporting decay times of 150 ms containing 9% of the signal and larger than 5% at 6 ms as has been reported by Gobain (2018). It must be realised that afterglow measurements strongly depend on crystal quality, temperature, exposure dose and exposure time, therefore experimental results are hard to generalise. Although the response and the wavelength dependence on sensitivity of the photodiode and the PMT are slightly different, the measurement gives an indication about the effect of afterglow on the PMT response in case of x-ray exposure.

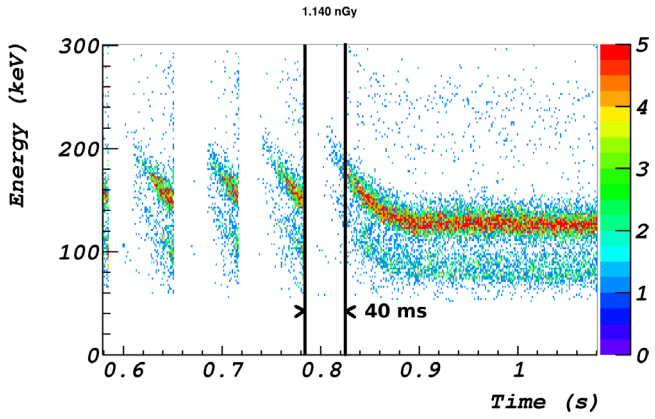

Figure 14. 2D histogram showing energy versus time of the last four x-ray pulses out of a burst of nine. Each pulse contains an x-ray dose of about 1.14 nGy. During the x-ray pulses the gamma camera seems to be blinded, in between the x-ray pulses excessive energies and a reduced count rate can be seen.

4.2. PMT response to a LED pulse

Figure 4 shows that exposure to 10 ms red LED pulses causes a sudden decrease in the dynode voltages and a sudden increase after the pulse ended. Both discharge and charge-up time seem to be significantly faster in case of small capacitors. This suggests that both are predominantly determined by the RC time, indicating a charge up of about 64% in 5 ms for 10 nF capacitors and a factor 10 faster in case of 1 nF capacitors. The presence of (partly) discharged capacitors shortly after the pulse ends, results in a decreased energy as can be seen for all curves in figure 6. Different from the 600 V curves, the 500 V curves show a maximum after a few milliseconds. This effect is believed to be caused by overlinearity (Photonis 2002). Overlinearity can be explained as follows: when the cathode voltage is fixed by the power supply, a decrease in potential across the last few dynodes results in an increase across all other dynodes causing a rising gain, leading to high measured energies. This effect is caused by discharging capacitors, hence its timescales are of the order of the capacitor charge-up time i.e. about 5 ms in case of 10 nF capacitors. This is in agreement with figure 4, which suggests that the dynode voltages restore faster with decreased capacitors.

The above results were obtained by subtraction of the probed responses from the unprobed responses. This method acts as an ideal high pass filter that offline selects the gamma pulses from the afterglow contribution. Implementation of an electronic high pass filter in the analogue PMT circuitry may perform the filtering online, such that the selection is done instantaneously.

4.3. NaI(Tl)-PMT assembly response to x-ray pulse

Any differences in response between the 10 ms LED pulse experiments and x-ray experiments are caused by the physical processes of the x-ray pulse interaction. The tails in figure 7 (1 nGy x-ray pulses) indicate that crystal afterglow time scales convolve with the capacitor charge-up time causing a longer recovery time. Moreover, when the next pulse occurs before complete charge-up, the capacitor charge-up relaxes until a steady state is reached. Although the behaviour in the tails is slightly different, the curves in figure 7 are consistent with the curves in figure 4 and the effect of afterglow on the performance is expected to be small. This is illustrated by figure 8, it can be seen that in between the pulses the energy curves are consistent with the response in case of absence of afterglow (figure 6), suggesting that the effect of afterglow on the energy measurements after baseline subtraction is small.

The fits in the figure 10 indicate that decay times of the curves are about 67 ms and are dose independent. For 9 nGy pulses the tails in the dynode voltage curves (figure 9) are more dominant, leading to a significant reduction in performance. Figure 11 shows that the reconstructed energies are heavily affected. The presence of afterglow on itself already causes the PMT to saturate in case of −600 V. Although the effects can be reduced by decreasing the gain, deterioration due to intense afterglow cannot be avoided.

4.4. Gamma camera response to x-ray pulse burst

Exposure of the gamma camera to intense x-ray pulses results in artefacts causing significant bias in the energy measurements and count rate reduction between the pulses, possibly also affecting position measurements. These effects reduce with decreasing dose: from 0.02 nGy per pulse and lower the effects vanish (figure 12); the ^{57}Co event rate remains constant and the reconstructed energy is as expected. The artefacts as observed beyond 0.02 nGy per pulse are presumably dominated by the presence of saturation effects in the PMTs, afterglow of the crystal and the gamma camera event processing system. One possible explanation for the increased energies is

that the afterglow contributes to the gamma light pulse, resulting in elevated reconstructed energies. The decay time of 50 ms, as extracted from figure 13, is smaller than what has been found in the previous measurements. It may be, that the event processing system affects these time scales. Although the decay times as observed with the gamma camera, the decay times as measured with a single NaI(Tl)-PMT assembly and the decay times as measured with the photodiode are comparable, much larger x-ray doses can be handled by the single NaI(Tl) assembly without losing counts.

4.5. Dose reduction methods

It has been demonstrated, that the performance of a conventional gamma camera is severly deteriorated when exposed to x-ray pulse doses of larger than about 0.02 nGy. In practice, nuclear images are acquired with a gamma camera-collimator assembly. It strongly depends on the collimator geometry and its orientation to what x-ray dose the gamma camera is exposed, hence a modification in orientation or geometry may be used to reduce the x-ray dose. In addition, attenuation filters may be used to reduce the x-ray flux. For instance, a 0.5 mm Tin filter after a phantom (20 cm of water) may be used to reduce the x-ray flux (80 kVp) by about an order of magnitude, at the cost of losing one fifth of 140 keV gammas.

5. Implementation

The PMT measurements suggest that modification of the PMT analogue circuitry and subtraction of the relatively constant afterglow component can be used to reduce deteriorating effects of afterglow on gamma energy measurements. The subtraction step may be avoided by the introduction of a high pass filter with a cut-off frequency above the primary NaI(Tl) decay time (250 ns (Gobain 2018)), but well below the dominant afterglow time components in our application (54 ms) e.g. in the range of 10–100 kHz. This may be a passive, an active or a digital high pass filter. However, the choice of type and cut-off frequency, may affect the performance of the PMT. This, together with the application of the findings in conventional gamma cameras during simultaneous hybrid nuclear and x-ray imaging, should be studied in more detail.

6. Conclusion

Afterglow of the scintillation crystal and limitations in PMT performance may significantly hamper gamma camera operation during and after x-ray exposure.

It has been demonstrated that modification of the PMT decoupling capacitances to 1 nC reduces the electronic effects after x-ray expose to time scales less than a few ms, which is acceptable for our hybrid imaging application. Furthermore, the effect of afterglow on gamma energy measurements can be reduced by subtraction of the independently measured afterglow contribution. However, this method is successful up to 1 nGy x-ray pulses, beyond this value the voltage drop across the dynodes starts to dominate the gain and introduces an undesired time dependency.

In addition it has been shown that a conventional gamma camera is limited in performance shortly ($\tau \approx 50$ ms) after x-ray pulse exposure, with doses larger than 0.02 nGy per pulse.

Acknowledgments

We would like to thank Scionix, Bunnik, and Philips Healthcare, Best, for their support to this research.

This work is part of the STW-VIDI research programme with project number 12977, which is (partly) financed by the Netherlands Organisation for Scientific Research (NWO).

This project has received funding from the European Research Council (ERC) under the European Union's Horizon 2020 research and innovation programme (grant agreement No [646734]).

ORCID iDs

S van der Velden https://orcid.org/0000-0002-8054-0175

References

Beijst C *et al* 2016 Toward simultaneous real-time fluoroscopic and nuclear imaging in the intervention room *Radiology* **278** 232–8
Braat A J A T *et al* 2015 90Y hepatic radioembolization: an update on current practice and recent developments *J. Nucl. Med.* **56** 1079–87
Cherry S, Sorenson J and Phelps M 2012 *Physics in Nuclear Medicine* (Amsterdam: Elsevier)
Gobain S 2018 www.crystals.saint-gobain.com/
Knoll G F 2000 *Radiation Detection and Measurement* 4th edn (New York: Wiley)
Kobayashi K *et al* 2012 Image-guided biopsy: what the interventional radiologist needs to know about PET/CT *Radiographics* **32** 1483–501

Koički S *et al* 1973 The investigation of the 0.15s phosphorescent component of NaI(Tl) and its application in scintillation counting *Nucl. Instrum. Methods* **108** 297–9
Hamamatsu Photonics K.K 2007 *Photomultiplier Tubes Basics and Applications 3a* (Hamamatsu: Hamamatsu Photonics K.K)
Photonis 2002 *Photomultiplier Tubes: Principles and Applications* (Brive: Photonis)
ET Enterprises 2010 PMT 9266B Data Sheet (Sweetwater, TX: ET Enterprises) (http://my.et-enterprises.com/pdf/9266B.pdf)
Raj S *et al* 2013 C-arm cone beam computed tomography: a new tool in the interventional suite *Ann. Acad. Med. Singap.* **42** 585–92 (PMID: 24356655)
Rodnyi P A 1997 *Physical Processes in Inorganic Scintillators* (New York: CRC)
Shyn P B 2013 Interventional positron emission tomography/computed tomography: state-of-the-art *Tech. Vasc. Intervent. Radiol.* **16** 182–90
van der Velden S *et al* 2017 Estimation of lung shunt fraction from simultaneous fluoroscopic and nuclear images *Med. Phys.* **44** 249–61
Vidal-Sicart S *et al* 2014 Contribution of perioperative imaging to radioguided surgery *Q. J. Nucl. Med. Mol. Imaging* **58** 140–60 (PMID: 24835290)